JOURNAL OF GEOPHYSICAL RESEARCH, VOL. 115, D05201, doi:10.1029/2009JD012689, 2010

Simulations of the effects of surface heat flux anomalies on stratification, convective growth, and vertical transport within the Saharan boundary layer

Qian Huang,[1] John H. Marsham,[2] Douglas J. Parker,[2] Wenshou Tian,[1] and Christian M. Grams[3]

Received 19 June 2009; revised 23 September 2009; accepted 5 October 2009; published 4 March 2010.

[1] Using two cases based on observations from the Geostationary Earth Radiation Budget Intercomparison of Longwave and Shortwave Radiation field campaign, large eddy model (LEM) simulations have been used to investigate the effects of surface flux anomalies on the growth of the summertime Saharan convective boundary layer (CBL) into the Saharan Residual Layer (SRL) above and transport from the CBL into the SRL. Hot surface anomalies generated updrafts and convergence in the CBL that increased transport from the CBL into the SRL. The induced subsidence in regions away from the anomalies inhibited growth of the CBL there. If the domain-averaged surface fluxes were kept constant, this led to a shallower, cooler CBL. If fluxes outside the anomalies were kept constant so that stronger anomalies led to increased domain-averaged fluxes, this gave a warmer, shallower CBL. These effects were larger for wider, stronger anomalies with low winds. The low-level wind speed variations induced by the anomalies were also shown to affect dust uplift rates. Previous observations have shown that the summertime SRL, which often contains sublayers of varying humidity and dust content, can persist until late in the afternoon. The LEM simulations presented show that mesoscale variations in surface fluxes can contribute both to inhibiting the growth of the Saharan CBL into the SRL and to generating layerings within the SRL.

Citation: Huang, Q., J. H. Marsham, D. J. Parker, W. Tian, and C. M. Grams (2010), Simulations of the effects of surface heat flux anomalies on stratification, convective growth, and vertical transport within the Saharan boundary layer, *J. Geophys. Res.*, *115*, D05201, doi:10.1029/2009JD012689.

1. Introduction

[2] Mineral dust plays an important role in the climate [*Intergovernmental Panel on Climate Change*, 2007] (available at http://www.ipcc.ch/ipccreports/ar4-wg1.htm), and the Sahara Desert is the world's largest source of mineral dust [*Tanaka and Chiba*, 2006]. Dust is uplifted from the desert surface into the Saharan boundary layer. It can then be exported over the surrounding colder, shallower boundary layers in a dry layer known as the Saharan Air Layer (SAL). In the SAL, significant quantities of dust can avoid rain-out over the Atlantic Ocean, and the dust can travel thousands of kilometers, even affecting the biology of the Amazon rain forest [e.g., *Talbot et al.*, 1986].

[3] The very large surface sensible and very low latent heat fluxes in the Sahara Desert lead to its unusually deep, almost dry-adiabatic boundary layer, which often reaches 6 km [*Gammo*, 1996]. This is often observed to consist of a shallow convective boundary layer (CBL) with a near-neutral residual layer above (the Saharan Residual Layer, or SRL). Multiple near-neutral layers are frequently observed within the SRL or within the SAL [*Parker et al.*, 2005; *Flamant et al.*, 2007; *Marsham et al.*, 2008a, 2008b], each with a different water vapor content and each separated by a weak lid (e.g., Figure 1). A local maximum in not only relative humidity, but also the water vapor mixing ratio (WVMR) is often seen at the top of the SRL or SAL [*Flamant et al.*, 2007] (Figure 1, case 1), where a layer of cumuliform clouds (broken or stratiform) is often observed to form [*Parker et al.*, 2005]. This structure suggests that in some locations, at some times, convection from the surface is mixing the full depth of the Saharan boundary layer, but at most locations and times, this is not the case, and varying horizontal advection leads to the multiple layering observed. This process is not well evaluated or understood, however, and until recently, there have been very few observations available from this region. In particular, the frequency of occurrence of the high WVMR layer at the top of the SRL is not well quantified nor its mechanism of generation well explained. The boundary layer schemes of global models are generally not designed to represent such deep dry

[1]Key Laboratory for Semi-Arid Climate Change of the Ministry of Education, College of Atmospheric Sciences, Lanzhou University, Lanzhou, China.
[2]National Centre for Atmospheric Science, School of Earth and Environment, University of Leeds, Leeds, UK.
[3]Institut für Meteorologie und Klimaforschung, Forschungszentrum Karlsruhe, Universität Karlsruhe, Karlsruhe, Germany.

0148-0227/10/2009JD012689$09.00

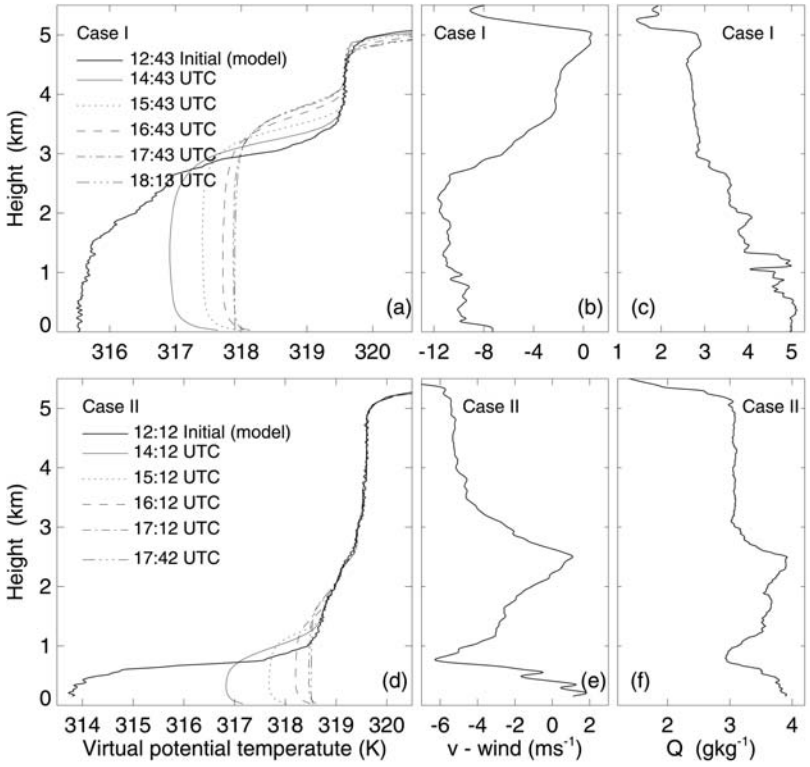

Figure 1. Simulated profiles of virtual potential temperatures (θ_v) from 2-D runs with no surface flux anomalies, initialized with dropsondes at (top) 1243 UTC (case 1) and (bottom) 1212 UTC (case 2). Bold lines show the observed (initial model) profiles of (a, d) θ_v, (b, e) westerly (v-wind) wind, and (c, f) water vapor mixing ratio (Q).

convection, and *Vuolo et al.* [2009] showed that multiple dust layers in the Saharan boundary layer are more common in satellite-borne lidar data than in their regional model.

[4] The Geostationary Earth Radiation Budget Intercomparison of Longwave and Shortwave Radiation (GERBILS) field campaign took place in the western Sahara during June 2007 and aimed to understand the difference in outgoing longwave radiation observed between a global model and satellite data [*Haywood et al.*, 2005]. The multilayered structure of the SRL and SAL was frequently observed during GERBILS, not only in buoyancy and WVMR, but also in dust content [e.g., *Marsham et al.*, 2008a, Figure 5; *Marsham et al.*, 2008b, Figure 3]. Using aircraft data from GERBILS, *Marsham et al.* [2008a] showed that land surface temperature (LST) anomalies with scales of 10 km or more were observed to affect the buoyancy and winds in the Saharan CBL, even on a day with significant winds (4 m s^{-1} along the aircraft track and a wind speed of 10 m s^{-1}). At 1300 UTC on this day, a rocky area approximately 20 km across, with an albedo of approximately 0.2, compared with 0.45 for the surrounding desert, was linked to a CBL temperature increase of approximately 2 K. Since the SRL is so weakly stratified, such variations may significantly affect the vertical mixing of the SRL, but no observations from the SRL were available in this case [*Marsham et al.*, 2008a].

[5] Although the authors are unaware of any other modeling studies of the impacts of land surface heterogeneity on the Saharan boundary layer, there is a large existing body of literature about impacts of land surface variations on other CBLs. These variations can arise from, for example, soil moisture or vegetation [e.g., *Beyrich et al.*, 2006] or albedo. Soil thermal properties and soil moisture have been shown to affect the partitioning between surface and sensible fluxes from the land to the atmosphere, affecting boundary layer properties and circulations (e.g., see *Kang et al.* [2007] for the continental United States). Albedo variations affect the net solar radiation warming the surface, and so the boundary layer [e.g., *Wendt et al.*, 2007], and even moving cloud–induced variations in net solar radiation at the surface, have been shown to generate mesoscale circulations [*Marsham et al.*, 2007a, 2007b]. To the south of the Sahara, in the Sahel, the combination of initially dry soils, sparse vegetation, and intense, localized precipitation can lead to significant soil moisture–induced circulations [*Taylor et al.*, 2003, 2007]. In the central Sahara, the albedo is variable [*Moody et al.*, 2005; *Houldcroft et al.*, 2009; *Marsham et al.*, 2008a; *Bierwirth et al.*, 2009], but vegetation is minimal, and away from regions affected by rare rain events, the soil moisture is very low. Therefore, the impacts of variations in albedo (and orography) are expected to dominate the impacts from soil moisture and vegetation. This is consistent with the results of *Marsham et al.* [2008a], who observed significant coherence between albedos and radiometric land surface temperatures on scales between 2.5 and 50 km. Albedos derived from satellite data show that albedo variations occur across the Sahara on a wide variety of scales [e.g., *Marsham et al.*, 2008a, Figure 3a].

[6] *Mahrt* [2000] provide a useful overview of the impacts of surface heterogeneities on the vertical structure

of boundary layers, in particular highlighting the limitations of the flux aggregation (tile or Mosaic approach) to parameterization of subgrid heterogeneity in models. The dependence of boundary layer responses on the scale of surface heterogeneity is complex and incompletely understood, but the strongest effects on boundary layer properties typically tend to occur on spatial scales of 2–20 km [*Mahrt*, 2000; *van Heerwaarden and de Arellano*, 2008]. However, this is expected to be larger for the Saharan CBL, which can be among the deepest on Earth, since both *Patton et al.* [2005] and *Dalu et al.* [1996] show that the effects scale with the boundary layer depth (with *Patton et al.* [2005] showing maximum impacts for 4–9 times the CBL depth). *Avissar and Schmidt* [1998] discuss how impacts also depend nonlinearly on the mean heating rate as well as on the background winds and anomaly scales, with greater effects for lower heating rates, but this is poorly understood [*Mahrt*, 2000]. In addition, *Letzel and Raasch* [2003] show that larger anomalies (greater than 5 km in their case) can generate temporal oscillations in the boundary layer. The work of *Patton et al.* [2005] differs from the other studies discussed in that the authors used a land surface model with two-way coupling with a large eddy model (LEM), rather than imposing surface fluxes or temperature variations at the land surface in the LEM. They simulated a grass-covered land surface with striped soil moisture patches and zero mean initial wind. They showed that the circulations induced by surface patches reduced the fluxes in the middle of the patches compared with their edges since the induced wind speeds were lower over the middle of the patches. For scales of surface flux variations greater than approximately 18 times the CBL depth, this allowed flux gradients within patches to overcome gradients between patches, allowing the coexistence both of smaller cells within the patches and larger-scale patch-induced variations.

[7] Dust uplift is a nonlinear function of wind speed (generally parameterized as a function of wind speed cubed, with a threshold wind speed [e.g., *Cakmur et al.*, 2004; *Marticorena and Bergametti*, 1997]), so fluctuations in wind speed (in time or space) can significantly affect dust uplift. As a result of this nonlinearity, some studies have shown that boundary layer convection can make a significant contribution to the winds that result in dust uplift in the Sahara [e.g., *Cakmur et al.*, 2004], and observations of *Marsham et al.* [2008a] showed that the LST anomalies affect the winds in the boundary layer. Therefore, such LST anomalies are expected to affect dust uplift.

[8] The observations from the African Monsoon Multidisciplinary Analysis and other projects in Africa have led to some overall understanding of the Saharan boundary layer and its interactions with African weather and climate. For example, in recent years, simulations have shown how the Saharan Heat Low (SHL) acts as a control on the onset of the West African Monsoon [*Sultan and Janicot*, 2003; *Drobinski et al.*, 2005; *Ramel et al.*, 2006; *Sijikumar et al.*, 2006; *Lavaysse et al.*, 2009]. However, the quality of model representation of the thermodynamic processes over the Sahara remains uncertain, and effects of spatial variations in the heat flux over the desert surface on the boundary layer energy and mass transport are still a subject of much interest.

[9] In this study, we use LEM simulations to investigate the effect of surface heat flux anomalies on the Saharan boundary layer (section 2). The authors are not aware of any other LEM simulations of the boundary layer of the Sahara, which exhibits the deepest dry convection on Earth [*Gammo*, 1996], although *Takemi et al.* [2006] presents LEM simulations of a 4 km deep boundary layer over the Gobi Desert of China, using spatially uniform surface fluxes. Our main focus is on the impacts of surface flux anomalies on the mean profile of the Saharan boundary layer (section 3.1) and on the vertical transport from the CBL into the SRL (section 3.2). Section 3.3 briefly examines the effects of the anomalies on dust uplift from the land surface under varying ambient wind conditions. Section 4 summarizes and discusses our findings.

2. Case Studies, Model Setup, and Method

[10] The model used is the U.K. Met Office LEM [*Gray et al.*, 2001]. Two cases were simulated, each initialized using a dropsonde profile from 24 June 2007, made during the GERBILS field campaign. Case 1 was initialized with a profile from 18°N, 8.7°W at 1243 UTC, and case 2 was initialized with a dropsonde from 18°N, 5.7°W at 1212 UTC. These were therefore both from a similar region of the southern Sahara, but the profiles differed due to different effects from the monsoon and the baroclinic zone at the western edge of the Sahara [*Grams et al.*, 2009] in each case.

[11] Two-dimensional (y-z) simulations were performed since a significant number of runs over extensive domains were required (sensitivity tests using three dimensions and smaller grid spacings than these standard runs were also performed, as described later). The model domain was 8 km deep, and the horizontal domain length was 200 km for case 1 runs and 100 km for case 2 runs (sensitivities to domain size are discussed in section 3.1). A horizontal grid spacing of 200 m was used, with a vertically stretched grid having a minimum spacing of 50 m in the boundary layer and a maximum of 150 m above 5 km. Periodic lateral boundary conditions were used. To reduce the reflection of internal gravity waves, a Newtonian damping layer was applied above 5300 m (a sensitivity study in which this was increased to 5700 m showed that this had negligible impact). As is usual for LEM simulations, at the start of a run, random perturbations (of ±0.2 K and 0.05 g kg^{-1}) were added to temperature and WVMR fields below 1000 m to allow boundary layer convection to develop in the model [*Gray et al.*, 2001; *Huang et al.*, 2009].

[12] The model surface heat flux was provided by the Consortium for Small-Scale Modeling model [*Doms and Schättler*, 2002] (available at http://www.cosmo-model.org) from the Deutscher Wetterdienst, which was run operationally during GERBILS and has been evaluated using aircraft data from 24, 27, and 28 June [*Grams et al.*, 2009; *Marsham et al.*, 2008a, 2008b]. These studies showed that the model captured the main structures observed well, but not the details of all the layerings observed in the SAL and SRL.

[13] It is known that the effect of surface heat flux anomalies on the CBL depends on both the spatial scales of anomalies and background wind conditions [e.g., *Hadfield et al.*, 1991]. However, this has not previously been investigated for the unusually deep boundary layer of the Sahara. Therefore, in this study, a range of simulations with different

Table 1. Parameters Varied for Cases 1 and 2 for Simulations Using Different Magnitudes of Surface Flux Anomaly (M), Scales of Surface Anomaly (D), and Ambient Wind Speeds at the Height of 1 km (U)

Case	Anomalies M	Scale D (km)	Wind Speeds U (m s^{-1})
Case 1	1.25	20	2.0
	1.75	30	5.0
	2.25	40	10.0
	2.5	50	15.0
	3.0	60	20.0
Case 2	1.25	5	2.3
	1.75	10	4.5
	2.25	20	9.0
	2.5	30	13.5
	3.0	40	22.5

spatial scales of heat flux anomalies under different ambient winds have been performed. A small warm patch was located in the middle of the model domain, with its width varying from 20 to 60 km in case 1 and 5 to 40 km in case 2. Surface heat flux anomalies of different magnitudes are applied within this warm patch, under various ambient winds. Here "heat flux" refers to both the sensible and latent fluxes, although owing to the high Bowen ratio in the Sahara, the latter affects the results very little.

[14] Two 3-D simulations were run as sensitivity studies. These were for case 2 and used a 100 × 10 km domain with the surface flux anomaly applied over a 20 km wide strip extending the full 10 km width of the domain in the third dimension. In one run, no initial mean wind was applied in the third dimension. In the other, the observed wind was used. As discussed in section 3, the differences in both the mean potential temperature profile and tracer transport between results from these 3-D runs and the equivalent 2-D run were small. This supports the idea that the results from the 2-D simulations can be viewed as representing the effects of a linear anomaly in a 3-D domain (similar to the rocky valley and escarpment observed by *Marsham et al.* [2008a]). Three higher-resolution runs were also performed as sensitivity studies. The first two used a higher vertical resolution (a minimum grid spacing of 0.7 m in the surface layer and a maximum of 50 m above 5 km), with and without an anomaly (M = 2.25, D = 20 km, where M and D are introduced in equation (1)). The third used both this higher vertical resolution and a higher horizontal resolution (a grid spacing of 100 m), with an anomaly (M = 2.25, D = 20 km). As discussed in section 3, the effects of changing the resolution on the results presented were small.

[15] For the scales of land surface variations considered in this article (widths of 5 km or more), there is essentially a 1-D energy balance at the land surface between the net solar heating (controlled by the surface albedo) and the outgoing longwave, sensible heat flux into the atmosphere, sensible heat flux into the ground, and latent heat flux into the atmosphere (which, in the dry Sahara, is small). Therefore, surfaces of lower albedo result in an increased outgoing longwave flux and sensible heat fluxes into the air and ground. The precise magnitude of the increase of the sensible heat flux into the atmosphere depends on the two-way coupling between the land and the atmosphere, but to first order, it can be represented by a uniform increase in surface flux to represent a uniform albedo anomaly [*Patton et al.*, 2005]. This is most accurate for surface variations with "wavelengths" less than approximately 18 times the CBL depth, for which variations in fluxes between patches dominate those within the patch [*Patton et al.*, 2005]. The CBL depths in the simulations described in this article vary between approximately 1 and 4 km. Therefore, for this study, *Patton et al.* [2005] suggest that the two-way coupling is significant for simulations with anomalies of width greater than approximately 27 km (18 times a CBL depth of 2.5 km, with the anomaly wavelength taken as double the anomaly width). This includes the larger anomalies used in this article. However, this is a second-order effect, and *Patton et al.* [2005] show flux variations of only around 2% within a wet or dry patch. The effects of two-way coupling are also expected to be reduced in any simulations with a mean wind, and furthermore, unlike a wet soil surface that can dry in response to an induced low-level wind, in this study, the land albedo cannot evolve in response to the atmospheric circulations.

[16] Considering the 1-D energy balance arguments discussed earlier, to compare model results with observations, it makes sense simply to increase surface heat fluxes over the warm patch, as a representation of the low-albedo features which influenced the CBL during the GERBILS campaign (described by *Marsham et al.* [2008a]). However, when considering the consequences of an unresolved spatially varying heat flux for a global model, as well as from a theoretical perspective, it is useful to separate the effects of the total increase in heating from the effects of a localization of the heating. Therefore, for the majority of simulations, to keep the total heat flux into the modeled atmosphere a constant, a "balanced" surface heat flux approach is used, with reduced heating away from the warm patch. Therefore, if the surface heat flux over the domain without an anomaly is F, we define a nondimensional parameter M so that the heat flux (sensible and latent) over the warm patch is MF and the heat flux outside the warm patch is mF. For the balanced heat flux approach, m can determined by

$$m = \frac{L - MD}{L - D}, \tag{1}$$

where L and D are the model domain size and the anomaly width, respectively. M and m are the fractional increases and decreases of the surface heat flux over the warm patch and outside of the warm patch, respectively. Initial wind speeds were also varied from 0 to 5 times the observed value, and the wind speed at a height of 1 km is referred to as U. About 125 runs with different M, D, and U were performed in each case, and their control parameters are summarized in Table 1. All these runs used the balanced heat flux approach, unless stated otherwise. To investigate the effects of the surface heat flux anomalies on the transport from the CBL into the SRL, a passive tracer with a constant value of 100 was added at all levels below the 200 m model level in all simulations.

3. Model Results

3.1. Effects on the Boundary Layer

[17] Modeled horizontal-mean virtual potential temperature (θ_v) profiles from cases 1 and 2 are shown in Figures 1a

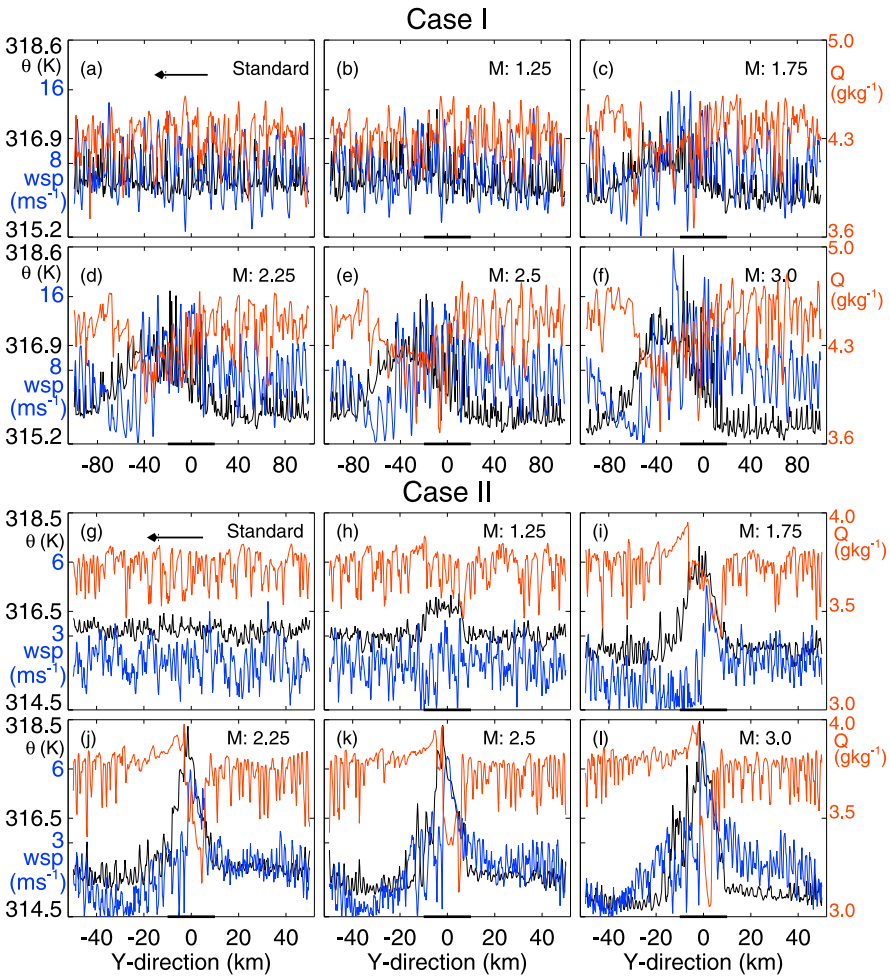

Figure 2. Potential temperatures (black), water vapor mixing ratio (Q, red), and wind speed (blue) at 344 m above ground level at 1443 UTC from (a) the standard run and the runs with M = (b) 1.25, (c) 1.75, (d) 2.25, (e) 2.5, and (f) 3.0, with 40 km wide surface anomalies in case 1; at 1412 UTC from (g) the standard run and the runs with M = (h) 1.25, (i) 1.75, (j) 2.25, (k) 2.5, and (l) 3.0, with 20 km wide surface anomalies in case 2. The mean CBL wind directions are represented by the arrows in Figures 2a and 2g.

and 1d. In both cases, the well-mixed CBL warms and deepens throughout the simulated time period (6 hours from 1243 UTC or 1212 UTC, respectively), and above this, there is a weakly stratified residual layer (the SRL), which extends up to approximately 5.0 km. In the SRL, layers with different WVMRs can be seen, often separated by weak inversions. The CBL is much shallower and cooler in case 2 than case 1, and this gives a quite different time development, with the CBL height reaching approximately 3.5 km for case 1 but only 1.8 km for case 2.

[18] The two 3-D simulations, initialized with 2-D and 3-D wind, respectively, gave very similar evolutions of the horizontal mean virtual potential temperatures as the equivalent 2-D simulation (not shown). This supports the use of 2-D simulations throughout the remainder of this study. There were small differences between the 2-D runs with decreased grid spacings and the equivalent lower-resolution 2-D run (not shown). Both higher-resolution runs gave slightly less entrainment, with CBLs that were approximately 150 m shallower than the 4 km deep CBL in the standard run. These differences suggest that the conclusions drawn from the large number of standard-resolution runs would be unaffected if it was possible to use the higher resolution for all runs.

[19] To investigate the effects of surface flux anomalies on the CBL, simulations were performed using the observed background wind speeds and constant anomaly size (40 km in case 1 and 20 km in case 2), but with varying strengths of the surface anomaly (M). Figure 2 shows potential temperature (θ, black lines), WVMR (Q, red lines), and horizontal wind speed (blue lines) at 344 m above ground level for runs initialized with the observed wind, 2 hours after the start of the simulation (1443 UTC for case 1 and 1412 UTC for case 2). This is from a similar altitude to the aircraft data shown in the work of *Marsham et al.* [2008a, Figure 4]. For both cases 1 and 2, as the anomaly strength is increased (from $M = 1$ to $M = 3$), the maximum θ in the CBL increases by approximately 1.5 K for case 1 and 2.1 K for case 2. The potential temperature increase is larger in case 2 because the perturbed fluxes converge within a shallower CBL in this case. Although neither case 1 nor case 2 is directly based on the observations of *Marsham et al.* [2008a] (where an

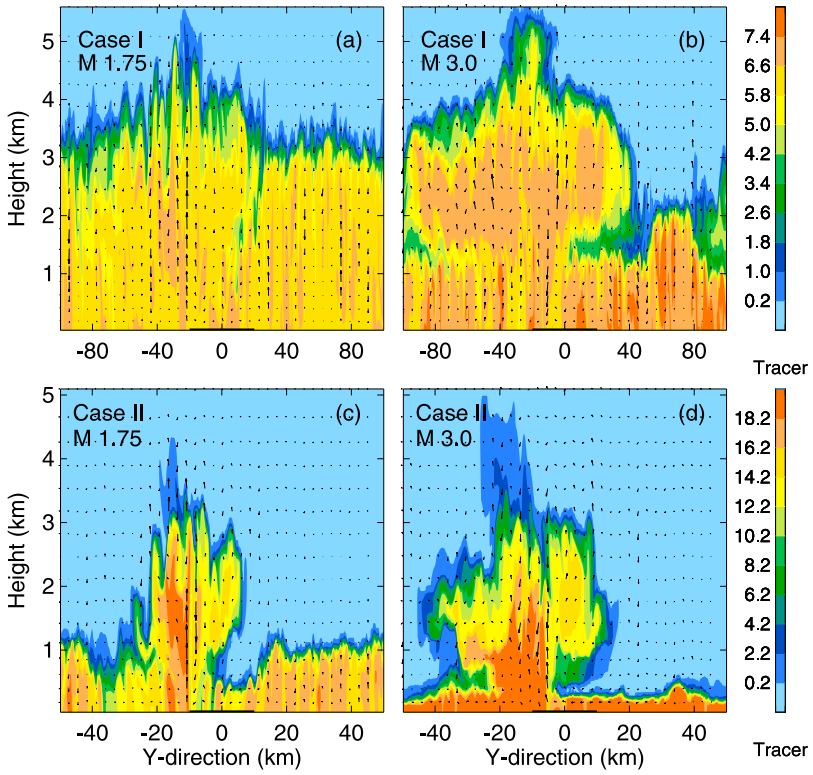

Figure 3. Instantaneous tracer and wind fields at 1813 UTC from case 1 runs with (a) M = 1.75 and (b) M = 3.0, with 0.2 times the observed wind, and at 1742 UTC from case 2 runs with (c) M = 1.75 and (d) M = 3.0, with 0.5 times the observed wind. Bold lines show the location of the warm surface anomaly.

observed profile was not available), the magnitude of the effects of the surface anomaly on the CBL in Figures 2i and 2j is broadly consistent with the aircraft observations of *Marsham et al.* [2008a]. Both the LEM and the aircraft observations show an increase of approximately 2 K over the width of the anomaly, for a similar-sized anomaly in similar conditions (along-track winds of approximately 4 m s^{-1}, a CBL depth of around 1 km, an anomaly width of 20 km, and with M = 1.75 or 2.25 in the LEM, and the albedo halved over the anomaly in the observations).

[20] There is convergence toward the high values of θ in the CBL. Initial wind speeds in the CBL are stronger for case 1 than case 2 ($\sim$10 m s^{-1} at 1 km compared with 4.5 m s^{-1}; see Figure 1), and so for case 1, the maximum values of θ (and associated convergence) are more clearly on the downwind (western, negative y) side of the surface anomaly (as shown by *Marsham et al.* [2008a]). The width of the high θ values is greater than the anomaly width in case 2 and more than twice the anomaly width in case 1, which is again consistent with the stronger CBL winds in case 1. The warm atmospheric anomalies tend to be dry, which must be from increased entrainment of dry air from above since the small latent heat fluxes are increased over the anomaly (consistent with the aircraft observations of *Marsham et al.* [2008a]). An enhancement of wind speed over the warm patch is also expected, from the downward transport of higher momentum by stronger convection over the warm patch.

[21] To further understand these modeled impacts of the surface flux anomalies, it is instructive to examine the 2-D model fields. Figure 3 shows winds and the passive tracer (which was initialized below 200 m). There is a strong updraft on the downwind (negative y) side of the anomalies, where maximum convergence occurs. This is coincident with a plume of tracer reaching higher altitudes than elsewhere in the domain: Remote from the plume, the tracer is contained in a much shallower CBL. For strong anomalies (Figures 3b and 3d), the tracer can be seen to have spread out laterally within the SRL. This has left a layer with lower tracer concentrations at altitudes between this detrained plume and the shallow CBL below (e.g., a layer of relatively low tracer concentration around 1.4 km altitude in Figure 3b). Similar plots of WVMRs (not shown) show that the anomalies also increase the entrainment of warm, dry air from the free troposphere into the SRL and also lead to greater specific humidities over the anomaly at all levels in the CBL. This second effect has the potential to enhance cloud formation, as discussed by *van Heerwaarden and de Arellano* [2008], but we have not investigated this process in detail. Away from the location of the anomaly (large positive and negative y), the stronger anomalies give a shallower CBL: As discussed in more detail later, this is due to a combination of the subsidence induced by the warm plume, the reduced surface fluxes in these regions (due to the balanced heat flux approach), the direct transport of air heated by the warm surface anomaly into the SRL, and the enhanced entrainment from the free troposphere into the SRL as a result of this. "Ogive curves," calculated using a running integral [*Friehe et al.*, 1991; *Brooks and Rogers*,

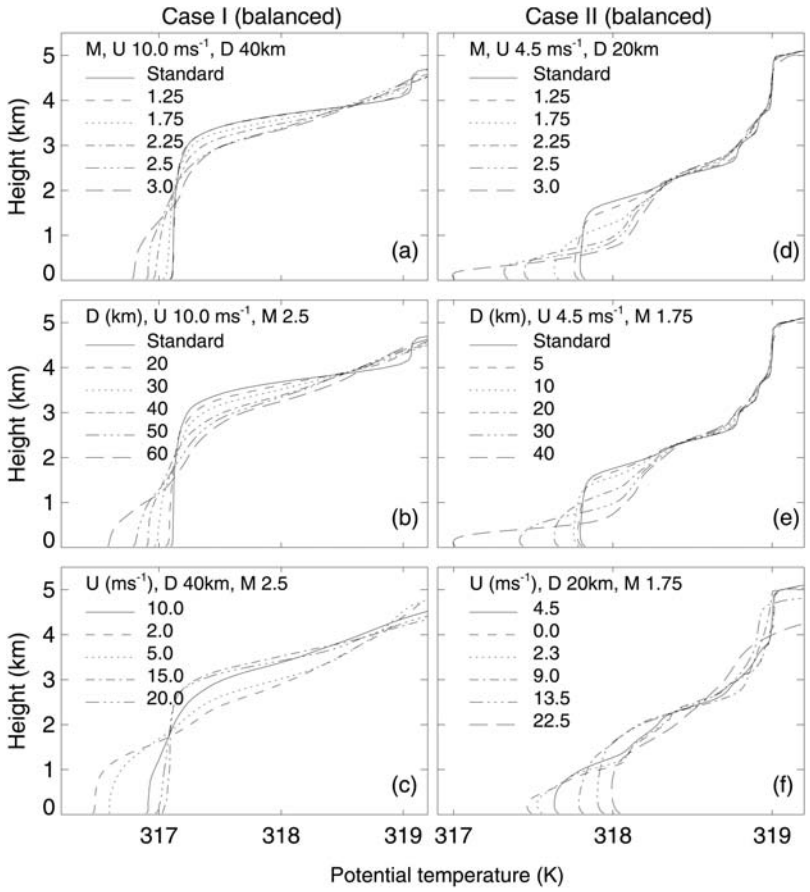

Figure 4. Vertical potential temperature profiles from runs using (a, d) different anomaly magnitudes (*M*), (b, e) different anomaly widths (*D*), and (c, f) different ambient wind speeds (*U*, illustrated by the wind speeds at the height of 1000 m). Results are from 1813 UTC for case 1 and 1742 UTC for case 2. All runs used balanced surface fluxes.

2000], were used to show the cumulative contribution to the fluxes from all wave numbers for runs with and without an anomaly (not shown). These confirmed that an anomaly of width 40 km and $M = 1.75$, with no initial wind, significantly increased the contribution of scales greater than 25 km to the fluxes at a height of 506 m in the convective boundary layer.

[22] To quantify the changes in CBL depth due to the warm surface flux anomaly, several simulations with different *M*, *D*, and *U* for cases 1 and 2 were performed. Figure 4 shows the horizontal-mean vertical profiles of potential temperature at the end of the simulations (1813 UTC for case 1 and 1742 UTC for case 2). Figures 4a and 4d show that for both cases, using balanced surface fluxes (thin lines), increasing *M* from 1.0 to 3.0 (while keeping *D* and ambient *U* fixed), leads to a shallower, cooler CBL (approximately 0.3 K cooler and 2 km shallower in case 1 and 0.9 K cooler and 1 km shallower in case 2). As already noted, this is due to a combination of increased subsidence and reduced surface fluxes away from the warm anomaly and direct transport of air warmed by the anomaly into the SRL. For unbalanced surface flux runs (Figure 5), for which the total heat flux into the modeled atmosphere is not a constant, the strong anomalies can still transport air from the CBL into the SRL and induce subsidence elsewhere. This still results in a shallower CBL, but this CBL is then warmer because away from the anomaly, the same surface fluxes are now heating a shallower CBL. In Figures 4 and 5, it can be seen that the mean CBL profile gets more stable as the anomalies are increased (this could also be seen in local profiles far from the anomaly and so is not merely an effect of the horizontal averaging). This is a similar result to that observed and modeled by *Kuwagata and Kimura* [1997] and *Bitencourt and Acevedo* [2008] for valley circulations (with and without a river), which they attributed to the subsidence that formed over the valley in their cases. As expected, increasing the width of the surface flux anomaly, while keeping its magnitude and ambient winds fixed (Figures 4b and 4e), has a similar effect as increasing *M*; wider anomalies give a shallower and cooler CBL (using the balanced heat flux approach).

[23] Because of the periodic lateral boundary condition of the LEM, simulations are essentially simulating an infinite series of similar anomalies, but for a small anomaly in a large domain, this is very close to simulating a completely isolated surface flux anomaly. The sensitivity to the domain size was investigated using case 2 for anomaly widths between 5 and 40 km. These were rerun using a 200 km domain instead of a 100 km domain. The comparison of horizontal potential temperatures in the CBL (at 238 m

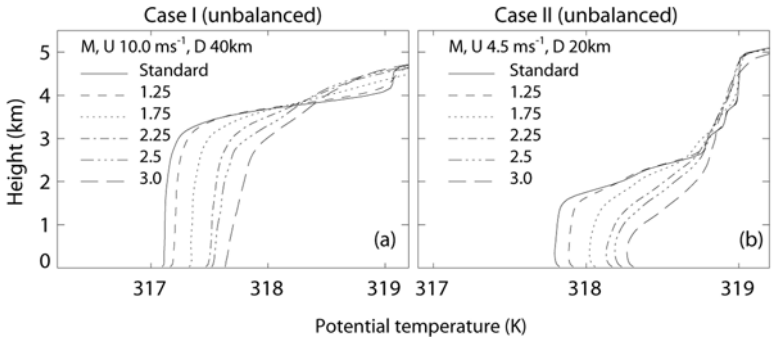

Figure 5. Same as Figures 4a and 4d, except all runs use unbalanced fluxes.

altitude) between 100 km and 200 km domain runs is shown in Table 2. For a fixed anomaly size, the larger domain reduces the effect of subsidence and increases the surface fluxes away from the anomaly (equation (1)). Both effects are expected to increase for an increasing anomaly size. This is confirmed by the LEM results, which show that for the larger domain, the mean temperatures in the CBL are approximately 0.5 K warmer for D = 40 km, 0.2 K warmer for D = 30 km, and 0.1 K warmer for D = 20 km, and effects are almost undetectable for D = 5 and 10 km. This is a two-thirds reduction in the effect of the anomaly on CBL temperatures for D = 40 km, and half for D = 20 km.

[24] Figures 4c and 4f show the effects of different ambient winds, with fixed D and M (D = 40 km for case 1 and 20 km for case 2, and M = 2.5 for case 1 and 1.75 for case 2). Stronger winds give a deeper, warmer CBL in both cases (600 m deeper and 0.1 K warmer, with U increasing from 10 m s^{-1} to 20 m s^{-1}, in case 1; 300 m deeper and 0.4 K warmer, with U increasing from 4.5 m s^{-1} to 22.5 m s^{-1}, in case 2); that is, strong winds decrease the impact of the warm anomaly on the surrounding CBL. Unlike the study of *Avissar and Schmidt* [1998], which showed no heterogeneity effects for wind speeds exceeding 5 m s^{-1}, the anomaly effects could be seen for all wind speeds. The strong winds decrease the time taken for the CBL air to be advected across the anomaly, and the stronger shear associated with the stronger winds is expected to increase mixing. Both effects give a less coherent plume above the surface flux anomaly, with more of the plume being mixed into the CBL, increasing the CBL temperature and decreasing the subsidence effects of the warm plume.

3.2. Effects on Transport Between the Convective Boundary Layer and Saharan Residual Layer

[25] Effects of surface flux anomalies have been shown to be greater for larger M or D. Figure 6 shows vertical distributions of the horizontally averaged passive tracer concentrations at different values of MD for runs with no ambient wind (note that the runs with D of 40 km in case 2 are eliminated in Figure 6 because of the large effects of the model lateral boundaries in those cases). Within 2 hours (Figures 6a and 6g), the tracer is essentially well mixed within the CBL (up to 2.1 km in case 1 and up to 900 m in case 2). This depth decreases with increasing MD as wider, warmer anomalies give a shallower CBL (section 3.1). More tracer is transported to higher maximum levels within the SRL with stronger anomalies (larger MD). For sufficiently large values of MD, this gives a clear vertical separation between the high tracer concentrations in the CBL and those from the detrained plume from the warm anomaly (e.g., for case 1 at 1813 UTC and MD = 160 km, the CBL tracer layer is 800 m deep and the detrainment layer is between 1.0 and 4.5 km, while for case 2 at 1742 UTC and MD = 90 km, the CBL tracer layer is 100 m deep and the detrainment layer is between 1 and 4 km). The altitude of the detrained plume increases with MD since the warmer, wider plumes can penetrate further into the SRL. Replotting Figure 6 for a single value of M (not shown) gave a smooth variation of the anomaly impacts with diameter. This and other results did not indicate any preferred anomaly size, which was shown by, for example, *Patton et al.* [2005].

[26] Vertical distributions of the horizontally averaged passive tracer concentrations at different values of MD/U (not shown) show that the effects of surface flux anomalies are greater for smaller U (we expect the effects of the anomaly generally to increase with increasing MD/U). The tracer does not reach as high as in Figure 6, owing to the effects of the wind. For both cases, for a given value of U, the amount of tracer that reached the upper levels of the SRL was found to increase approximately linearly with MD, but the relationship with MD/U was more complex (not shown). Again, differences between the 2-D simulation and 3-D simulation of case 2 (using M = 1.75 and D = 20 km) were small. The boundary layer tracer concentrations at the end of the simulations were approximately 10% greater in the 3-D run since the 3-D run gave a boundary layer that was approximately 10% shallower, and the two runs gave very similar transport of tracer to the free troposphere (not shown).

Table 2. Horizontal Mean Potential Temperature for Case 2 at 238 m Altitude With Different Scales of Surface Anomaly (D) and 4.5 m s^{-1} Ambient Wind Speed at the Height of 1 km at 1742 UTC for Standard Domain Size (L) of 100 km and Increased Size (L) of 200 km Runs

	D (km)				
$\theta(K)$	5	10	20	30	40
L = 100 km	317.78	317.75	317.63	317.42	317.04
L = 200 km	317.79	317.76	317.71	317.64	317.54

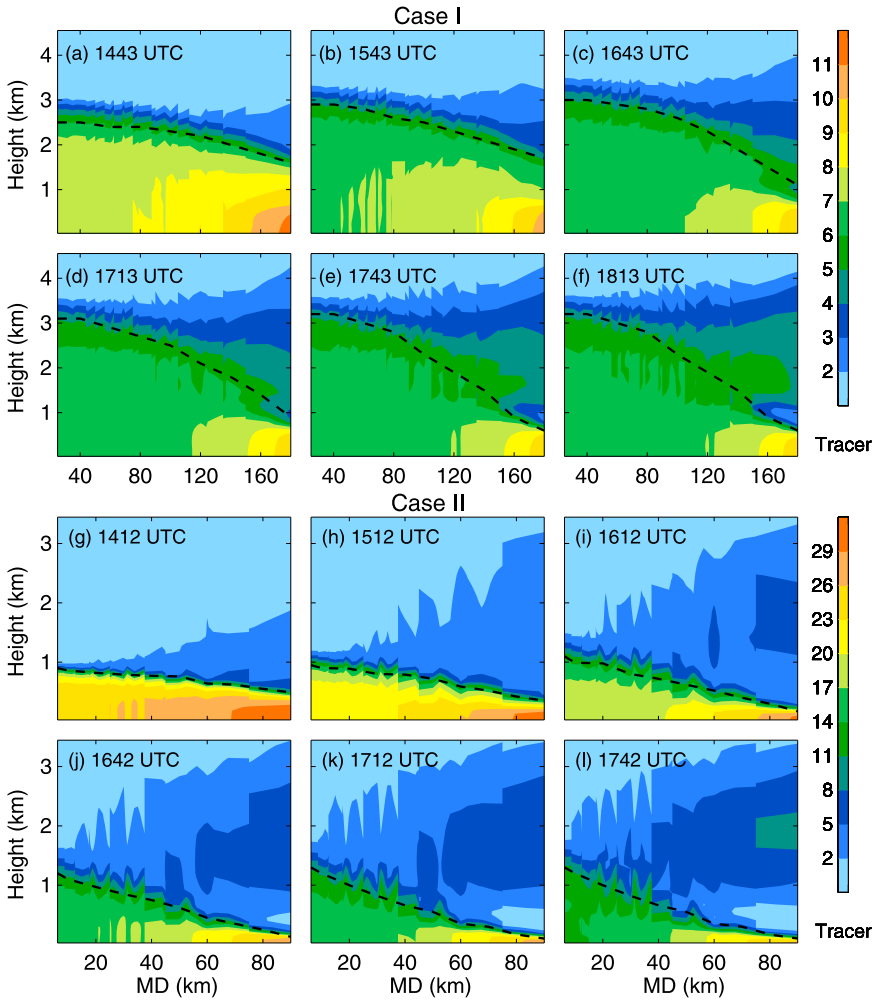

Figure 6. Horizontally averaged tracer as a function of height for different values of *MD* from runs using zero model ambient wind. Results are shown for case 1 at (a) 1443 UTC, (b) 1543 UTC, (c) 1643 UTC, (d) 1713 UTC, (e) 1743 UTC, and (f) 1813 UTC and for case 2 at (g) 1412 UTC, (h) 1512 UTC, (i) 1612 UTC, (j) 1642 UTC, (k) 1712 UTC, and (l) 1742 UTC, respectively. Dashed lines indicate the convective boundary layer depths.

[27] These results show that not only do stronger surface flux anomalies with lighter winds tend to decrease the CBL depth (using balanced or unbalanced surface fluxes), but they also enhance the vertical transport from the CBL into the SRL. Warm plumes located above the surface anomalies enhance transport from the CBL into the SRL and induce subsidence in the surrounding areas, inhibiting the CBL growth there. If an anomaly was sufficiently strong (or the lid between the CBL and SRL sufficiently weak), this could detrain air that was warmer than the SRL at the top of the SRL, stabilizing the SRL. This process would also enhance entrainment from the free troposphere into the SRL, which would further stabilize the SRL.

3.3. Effects on Dust Uplift From the Land Surface

[28] It is known that dust uplift occurs only for wind velocities higher than a threshold [*Gillette*, 1978], which is typically around 8–10 m s^{-1} in the Sahara [*Chomette et al.*, 1999] and is normally parameterized as a function of the friction velocity (u_*) cubed, with a threshold friction velocity [*Marticorena and Bergametti*, 1997; *Gillette*, 1978]. This nonlinear dependence of dust uplift on wind speed means that surface heat flux anomalies, which cause convergence in the boundary layer and affect the rate of downward mixing of momentum from above, might be expected to affect uplift rates.

[29] There is no dust model within the LEM, but in this section, we investigate the impacts of the surface anomalies on low-level winds to investigate their impacts on dust uplift. In the LEM,

$$u_* = k \cdot u_1/(\log(z/z_0) - \psi), \tag{2}$$

where u_1 is the wind velocity at the lowest model level, z_0 is the roughness length of the surface, k is the von Karman constant, and ψ accounts for stability. Therefore, for a constant surface roughness, if variations in ψ are neglected, u_* is proportional to u_1. A calculation of u_* with and without

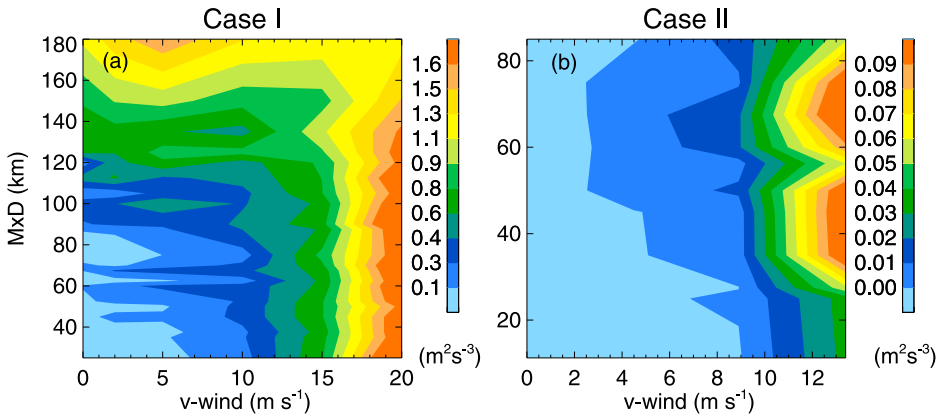

Figure 7. Mean "uplift rate" per meter (see text for details) as a function of the wind at 1 km (*v*-wind) and anomaly strength (*MD*). (a) Case 1 with $D = 40$ km at 1543 UTC and (b) case 2 with $D = 20$ km at 1512 UTC.

variations in ψ showed that variations in u_* were dominated by variation in u_1 (consistent with the work of *Marsham et al.* [2008a]). We therefore use variations in u_1 to investigate the impacts of the anomalies on dust uplift. We use *Cakmur et al.*'s [2004, equation (1)], which relates variations in dust uplift rate (F) to variations in low-level wind speed:

$$F \propto u^2(u - u_T), \tag{3}$$

for $u \geq u_T$, where u is the surface wind speed at 10 m and u_T is the threshold wind speed for uplift (as also used by *Marsham et al.* [2008a] for evaluating the effects of boundary layer convection within the LEM on dust uplift).

[30] In the LEM, we use the wind speed at the lowest model level (26 m) to calculate the dust uplift since our aim is only to investigate the sensitivity of uplift (i.e., averaged values of $u^2(u - u_T)$) to the anomalies, rather than model actual dust uplift rates (sensitivity tests using the higher-resolution 2-D runs showed that our results were robust to the vertical resolution used).

[31] Figure 7 shows the dependence of "uplift rates" (i.e., domain-averaged values of $u^2(u - u_T)$) for both cases, with varying anomaly strengths and ambient winds. Anomalies tend to increase dust uplift for low wind speeds both in cases 1 and 2, and especially in case 1, with wind speeds less than 15 m s^{-1}. For example, for case 1 with a mean wind of 10 m s^{-1}, an *MD* of 100 km increases uplift from approximately 0.3 to 0.6 m^2 s^{-3}. This occurs since the anomalies lead to locally increased wind speeds (see Figure 2) and uplift is a nonlinear function of wind speed cubed. Effects at higher wind speeds are reduced since the effect of the anomaly on CBL winds is then reduced.

[32] In reality, dust uplift rates depend on soil properties, moisture, and vegetation. As a sensitivity study, uplift rates were recalculated with dust only uplifted from outside the warm anomaly (since less dust uplift might be expected from a dark, rocky surface). This made the results more complex since the uplift was then sensitive to the location of the increased wind speeds with respect to the anomaly. In both cases 1 and 2, the effects were much less clear than in Figure 7, but there was perhaps a decrease in overall uplift rate for increasing anomaly strength (not shown), which must be a result of enhanced wind speeds over the anomaly and reduced wind speeds elsewhere (see Figure 2).

4. Summary and Discussion

[33] LEM simulations have been used to investigate the effects of surface flux anomalies on the growth of the Saharan CBL into the SRL and transport from the CBL into the SRL. Sensitivities to the scales and strengths of the anomalies (widths of 5–60 km and fluxes of 1–3 times the unperturbed values) as well as the ambient winds (0–5 times that observed) have been investigated. This work was motivated by the observational results of *Marsham et al.* [2008a], who showed that low albedo anomalies in the Sahara (on scales of 10 km or more) can lead to observable increases in land surface and CBL temperatures and to convergence in the CBL. However, *Marsham et al.* [2008a] could not evaluate the effects on the transport into the SRL since data were only available from within the CBL. The LEM simulations described in this article allow us to conclude that surface flux anomalies enhance modeled transport from the CBL into the SRL and inhibit the growth of the Saharan CBL.

[34] Two sets of LEM simulations were performed, each initialized with a dropsonde profile from the Saharan boundary layer, made during the GERBILS field campaign. A balanced surface flux approach was used, in which, as the anomaly strength increased, surface fluxes outside of the anomaly decreased to keep the domain-averaged flux constant. The effects of unbalanced fluxes (where the strength of the anomaly was simply varied) were also investigated. It would be interesting to extend this work by coupling a land model to the LEM to allow two-way coupling effects, which can be significant [*Patton et al.*, 2005]. However, we do not expect these two-way effects to significantly alter the conclusions from this article, and the balanced anomaly method used allows an idealization of the problem, maintaining a constant heat flux into the domain for all runs.

[35] Wider, stronger anomalies, with lighter winds, gave a shallower CBL away from the anomaly and enhanced transport of a tracer from the original CBL into the SRL above. This gave a cooler CBL with balanced surface fluxes but a warmer CBL with unbalanced fluxes. The results were

a consequence of the warm updraft over the surface flux anomaly, allowing air from the CBL to enter the SRL but generating subsidence elsewhere, which inhibited CBL growth. Stronger boundary layer winds gave a less coherent updraft over the surface anomaly and reduced these effects. A simulation of a 20 km strip (in the x direction) with an anomalous surface heat flux in a 3-D domain gave very similar results to the equivalent 2-D simulation. We can conclude that if it had been possible to use three dimensions for all runs, then this would not have significantly affected our results.

[36] These idealized modeling simulations provide valuable insights into observations from the Saharan boundary layer. Aircraft, dropsonde, and lidar profiles often show layering of dust and water vapor within the SRL [e.g., *Marsham et al.*, 2008a, 2008b], often with a maximum in WVMR at the top of the SRL [*Flamant et al.*, 2007]. *Vuolo et al.* [2009] showed that their regional model tends to underestimate the occurrence of multiple dust layers. The LEM simulations show that an anomaly in surface fluxes can generate such layering in the SRL (as shown toward the right-hand side of Figure 6). For a sufficiently strong anomaly, or weak inversion between the CBL and SRL, the simulations show how an anomaly could result in a plume that injects humid CBL air directly from the CBL into the top of the SRL (where it is stopped by the strong inversion between the SRL and the free troposphere). This would result in a WVMR maximum at the top of the CBL, as observed in some of the profiles of *Flamant et al.* [2007], and, by warming the top of the SRL, would further inhibit the growth of the CBL into the SRL.

[37] The CBL growth in the Sahara is known to be slow, with observations showing the SRL persisting until late in the afternoon. This persistence has important implications for the meteorology of the region and for dust transport. The LEM results show that surface flux anomalies suppress CBL growth away from the anomalies, contributing to the persistence of the SRL. Mountains in the Sahara (the Hoggar, Tibesti, etc.), which not only tend to be darker than the surrounding desert, but also provide an elevated heat source [e.g., *Tian and Parker*, 2003], are expected to generate stronger effects than simple surface flux anomalies.

[38] Although dust is not a prognostic variable in the LEM, the sensitivity of dust uplift from the land surface to anomalies was investigated by calculating an uplift rate as a cubic function of the low-level wind speed, with a threshold applied (as used by *Cakmur et al.* [2004] and *Marsham et al.* [2008a]). This showed that if the whole LEM domain had equal potential for dust uplift, then anomalies tended to increase uplift. This is a result of local variations in wind speed induced by the anomalies and the nonlinear nature of the uplift process. If the uplift could only occur outside of the anomaly, there was perhaps a decrease in overall uplift rate for increasing anomaly strength, but the results were much less clear. It would be interesting to add a full prognostic dust variable coupled to a radiation scheme in the LEM, allowing the dust radiative effects to feed back onto the boundary layer dynamics, but this was beyond the scope of this study.

[39] To capture these mesoscale processes, models must resolve them and use accurate albedos, or they must be parameterized. Failing to do this may have significant implications for the representation of the growth of the Saharan CBL into the SRL, the layering within the SRL, modeled meteorology, and dust transport.

[40] **Acknowledgments.** This work has been supported by the National Science Foundation of China (40730949) and the Doctorial Fund of the Ministry of China (20060730022). J.M. was supported by NERC grants NER/O/S/2002/00971 and NE/E006124/1, and D.P. was supported by NERC grant NE/B505538/1. Q.H. also thanks the School of Earth and Environment, University of Leeds, for computer support during this study. We gratefully appreciated Ian Brooks for useful discussions about calculating ogives of boundary layer fluxes. On the basis of a French initiative, AMMA was built by an international scientific group and is currently funded by a large number of agencies, especially from France, the United Kingdom, the United States, and Africa. It has been the beneficiary of a major financial contribution from the European Community's Sixth Framework Research Programme. Detailed information on scientific coordination and funding is available on the AMMA International Web site (http://www.amma-international.org). We would like to thank the three anonymous reviewers for their helpful comments, which improved the article.

References

Avissar, R., and T. Schmidt (1998), An evaluation of the scale at which ground-surface heat flux patchiness affects the convective boundary layer using large-eddy simulations, *J. Atmos. Sci.*, *55*, 2666–2689.

Beyrich, F., et al. (2006), Area-averaged surface fluxes over the LITFASS region based on eddy-covariance measurements, *Boundary Layer Meteorol.*, *121*, 33–65.

Bierwirth, E., et al. (2009), Spectral surface albedo over Morocco and its impact on radiative forcing of Saharan dust, *Tellus, Ser. B*, *61*, 252–269.

Bitencourt, D. P., and O. C. Acevedo (2008), Modelling the interaction between a river surface and the atmosphere at the bottom of a valley, *Boundary Layer Meteorol.*, *129*, 309–321, doi:10.1007/s10546-008-9318-6.

Brooks, I. M., and D. P. Rogers (2000), Aircraft observations of the mean and turbulent structure of a shallow boundary layer over the Persian gulf, *Boundary Layer Meteorol.*, *95*, 189–210.

Cakmur, R. V., R. L. Miller, and O. Torres (2004), Incorporating the effect of small-scale circulations upon dust emission in an atmospheric general circulation model, *J. Geophys. Res.*, *109*, D07201, doi:10.1029/2003JD004067.

Chomette, O., M. Legrand, and B. Marticorena (1999), Determination of the wind speed threshold for the emission of desert dust using satellite remote sensing in the thermal infrared, *J. Geophys. Res.*, *104*, 31,207–31,215.

Dalu, G. A., R. A. Pielke, M. Baldi, and X. Zeng (1996), Heat and momentum fluxes induced by thermal inhomogeneities with and without large-scale flow, *J. Atmos. Sci.*, *53*(22), 3286–3302.

Doms, G., and U. Schättler (2002), A description of the nonhydrostatic Regional Model LM. Part I: Dynamics and numerics, report, Consortium for Small-Scale Modell.

Drobinski, P., B. Sultan, and S. Janicot (2005), Role of the Hoggar massif in the West African monsoon onset, *Geophys. Res. Lett.*, *32*, L01705, doi:10.1029/2004GL020710.

Flamant, C., J. P. Chaboureau, D. J. Parker, C. M. Taylor, J. P. Cammas, O. Bock, F. Timouk, and J. Pelon (2007), Airborne observations of the impact of a convective system on the planetary boundary layer thermodynamics and aerosol distribution in the inter-tropical discontinuity region of the West African monsoon, *J. Atmos. Sci.*, *133*, 1175–1189.

Friehe, C. A., W. J. Shaw, D. P. Rogers, K. L. Davidson, W. J. Large, S. A. Stage, G. H. Crescenti, S. J. S. Khalsa, J. K. Greenhut, and F. Li (1991), Air-sea fluxes and surface layer temperatures around a sea-surface temperature front, *J. Geophys. Res.*, *96*, 8593–8609.

Gammo, M. (1996), Thickness of the dry convection and large-scale subsidence above deserts, *Boundary Layer Meteorol.*, *79*, 265–278.

Gillette, D. (1978), A wind tunnel simulation of the erosion of soil: Effect of soil texture, sand blasting, wind speed and soil consolidation on dust production, *Atmos. Environ.*, *12*, 1735–1743.

Grams, C. M., S. C. Jones, J. H. Marsham, D. J. Parker, J. M. Haywood, and V. Heuveline (2009), The Atlantic inflow to the Saharan heat low: Observations and modelling, *Q. J. R. Meteorol. Soc.*, doi:10.1002/qj.429.

Gray, M. E. B., J. Petch, S. H. Derbyshir, A. R. Brown, A. P. Lock, and H. A. Swann (2001), Version 2.3 of the Met. Office large eddy model, report, Met. Office, Exeter, U. K.

Hadfield, M. G., W. R. Cotton, and P. A. Pielke (1991), Large-eddy simulations of thermally forced circulations in the convective boundary layer, part I: A small-scale circulation with zero wind, *Boundary Layer Meteorol.*, *57*, 79–114.

Haywood, J. M., R. P. Allan, I. Culverwell, T. Slingo, S. Milton, J. Edwards, and N. Clerbaux (2005), Can desert dust explain the outgoing longwave radiation anomaly over the Sahara during July 2003?, *J. Geophys. Res.*, *110*, D05105, doi:10.1029/2004JD005232.

Houldcroft, C., W. Grey, M. Barnsley, C. Taylor, S. Los, and P. North (2009), New vegetation albedo parameters and global fields of background albedo derived from MODIS for use in a climate model, *J. Hydrometeorol.*, *10*, 183–198, doi:10.1175/2008JHM1021.1.

Huang, Q., J. H. Marsham, D. J. Parker, W. Tian, and T. Weckwerth (2009), A comparison of roll and nonroll convection and the subsequent deepening moist convection: An LEM case study based on SCMS data, *Mon. Weather Rev.*, *137*, 350–365, doi:10.1175/2008MWR2450.1.

Intergovernmental Panel on Climate Change (2007), 4th Assessment Report, Working Group I Report: The Physical Science Basis, Geneva. (Available at http://www.ipcc.ch/ipccreports/ar4-wg1.htm)

Kang, S. L., K. J. Davis, and M. LeMone (2007), Observations of the ABL structures over a heterogeneous land surface during IHOP_2002, *J. Hydrol. Meteorol.*, *8*, 221–244.

Kuwagata, T., and F. Kimura (1997), Daytime boundary layer evolution in a deep valley. Part II: Numerical simulation of the cross-valley circulation, *J. Appl. Meteorol.*, *36*, 883–895, doi:10.1175/1520-0450(1997)036<0883:DBLEIA>2.0.CO;2.

Lavaysse, C., C. Flamant, S. Janicot, D. J. Parker, J.-P. Lafore, B. Sultan, and J. Pelon (2009), Seaonal evolution of the West African heat low: A climatological perpective, *Clim. Dyn.*, *33*, 313–330, doi:10.1007/s00382-009-0553-4.

Letzel, M. O., and S. Raasch (2003), Large eddy simulation of thermally induced oscillations in the convective boundary layer, *J. Atmos. Sci.*, *60*, 2328–2341.

Mahrt, L. (2000), Surface heterogeneity and vertical structure of the boundary layer, *Boundary Layer Meteorol.*, *96*, 33–62.

Marsham, J. H., C. J. Morcrette, K. A. Browning, A. M. Blyth, D. J. Parker, U. Corsmeier, N. Kalthoff, and M. Kohler (2007a), Variable cirrus shading during CSIP IOP 5, part I: Effects on convective initiation, *Q. J. R. Meteorol. Soc.*, *133*, 1643–1660.

Marsham, J. H., A. M. Blyth, D. J. Parker, K. Beswick, K. A. Browning, U. Corsmeier, N. Kalthoff, S. Khodayar, C. J. Morcrette, and E. G. Norton (2007b), Variable cirrus shading during CSIP IOP 5, part II: Effects on the convective boundary layer, *Q. J. R. Meteorol. Soc.*, *133*, 1161–1675.

Marsham, J. H., D. J. Parker, C. M. Grams, B. Johnson, W. M. F. Grey, and A. N. Ross (2008a), Observations of mesoscale and boundary-layer scale circulations affecting dust transport and uplift over the Sahara, *Atmos. Chem. Phys.*, *8*, 6979–6993.

Marsham, J. H., D. J. Parker, C. M. Grams, C. M. Taylor, and J. M. Haywood (2008b), Uplift of Saharan dust south of the inter-tropical discontinuity, *J. Geophys. Res.*, *113*, D21102, doi:10.1029/2008JD009844.

Marticorena, B., and G. Bergametti (1997), Modelling of the atmospheric dust cycle: 2. Simulations of Sahara dust source, *J. Geophys. Res.*, *102*, 4387–4404.

Moody, E., M. King, S. Platnick, C. Schaaf, and G. Feng (2005), Spatially complete global spectral surface albedos: Value-added datasets derived from Terra MODIS land products, *IEEE Trans. Geosci. Remote Sens.*, *43*, 144–158.

Parker, D. J., C. D. Thorncroft, R. R. Buron, and A. Diongue-Niang (2005), Analysis of the African easterly jet, using aircraft observations from the JET2000 experiment, *Q. J. R. Meteorol. Soc.*, *131*, 1461–1482.

Patton, E. G., P. P. Sullivan, and C. H. Moeng (2005), The influence of idealized heterogeneity on wet and dry planetary boundary layers coupled to the land surface, *J. Atmos. Sci.*, *62*, 2078–2097.

Ramel, R., H. Gallee, and C. Messager (2006), On the northward shift of the West African monsoon, *CD*, *87*, 1739–1746.

Sijikumar, S., P. Roucou, and B. Fontaine (2006), Monsoon onset over Sudan-Sahel: Simulation by the regional scale model MM5, *Geophys. Res. Lett.*, *33*, L03814, doi:10.1029/2005GL024819.

Sultan, B., and S. Janicot (2003), The West African monsoon dynamics. Part II: The preonset and onset of the summer monsoon, *J. Clim.*, *16*, 3407–3427.

Takemi, T., M. Yasui, J. Zhou, and L. Liu (2006), Role of boundary layer and cumulus convection on dust emission and transport over a midlatitude desert area, *J. Geophys. Res.*, *111*, D11203, doi:10.1029/2005JD006666.

Talbot, W. R., R. C. Harriss, E. V. Browell, G. L. Gregory, D. I. Sebacher, and S. M. Beck (1986), Distribution and geochemistry of aerosols in the tropical North Atlantic troposphere: Relationship to Sahara dust, *J. Geophys. Res.*, *91*, 5173–5182.

Tanaka, T. Y., and M. Chiba (2006), A numerical study of contributions of dust source regions to the global dust budget, *Global Planet. Change*, *52*, 88–104.

Taylor, C. M., R. J. Ellis, D. J. Parker, R. R. Burton, and C. D. Thorncroft (2003), Linking boundary-layer variability with convection: A case-study from JET2000, *Q. J. R. Meteorol. Soc.*, *129*, 2233–2253.

Taylor, C. M., D. J. Parker, and P. P. Harris (2007), An observational case study of mesoscale atmospheric circulations induced by soil moisture, *Geophys. Res. Lett.*, *34*, L15801, doi:10.1029/2007GL030572.

Tian, W., and D. J. Parker (2003), A modelling study and scaling analysis of orographic effects on boundary layer shallow convection, *J. Atmos. Sci.*, *60*, 1981–1991.

van Heerwaarden, C. C., and J. V. de Arellano (2008), Relative humidity as an indicator for cloud formation over heterogeneous land surfaces, *J. Atmos. Sci.*, *65*, 3263–3277, doi:10.1175/2008JAS2591.1.

Vuolo, M. R., H. Chepfer, L. Menut, and G. Cesana (2009), Comparison of mineral dust layers vertical structures modeled with CHIMERE-DUST and observed with the CALIOP lidar, *J. Geophys. Res.*, *114*, D09214, doi:10.1029/2008JD011219.

Wendt, C. K., J. Beringer, N. J. Tapper, and L. B. Hutley (2007), Local boundary-layer development over burnt and unburnt tropical savanna: An observational study, *Boundary Layer Meteorol.*, *124*, 291–304.

C. M. Grams, Institut für Meteorologie und Klimaforschung, Forschungszentrum Karlsruhe, Universität Karlsruhe, D-76021 Karlsruhe, Germany.

Q. Huang and W. Tian, Key Laboratory for Semi-Arid Climate Change of the Ministry of Education, College of Atmospheric Sciences, Lanzhou University, Tianshui Rd., Lanzhou, Gan Su 730000, China. (qianhuang@lzu.edu.cn)

J. H. Marsham and D. J. Parker, National Centre for Atmospheric Science, School of Earth and Environment, University of Leeds, Leeds LS2 9JT, UK.